ARMY RESEARCH LABORATORY

ARL

Characterization of Next Generation Commercial Surface Enhanced Raman Scattering Substrates with a 633- and 785-nm System

by Mikella E. Farrell, Dimitra N. Stratis-Cullum, and Paul M. Pellegrino

ARL-TR-6419   **April 2013**

NOTICES

Disclaimers

The findings in this report are not to be construed as an official Department of the Army position unless so designated by other authorized documents.

Citation of manufacturer's or trade names does not constitute an official endorsement or approval of the use thereof.

Destroy this report when it is no longer needed. Do not return it to the originator.

Army Research Laboratory

Adelphi, MD 20783-1197

ARL-TR-6419   **April 2013**

Characterization of Next Generation Commercial Surface Enhanced Raman Scattering Substrates with a 633- and 785-nm System

Mikella E. Farrell, Dimitra N. Stratis-Cullum, and Paul M. Pellegrino
Sensors and Electron Devices Directorate, ARL

---

1. REPORT DATE *(DD-MM-YYYY)*	2. REPORT TYPE	3. DATES COVERED *(From - To)*
April 2013	Final	

4. TITLE AND SUBTITLE	5a. CONTRACT NUMBER
Characterization of Next Generation Commercial Surface Enhanced Raman Scattering Substrates with a 633- and 785-nm System	
	5b. GRANT NUMBER
	5c. PROGRAM ELEMENT NUMBER

6. AUTHOR(S)	5d. PROJECT NUMBER
Mikella E. Farrell, Dimitra N. Stratis-Cullum, and Paul M. Pellegrino	
	5e. TASK NUMBER
	5f. WORK UNIT NUMBER

7. PERFORMING ORGANIZATION NAME(S) AND ADDRESS(ES)	8. PERFORMING ORGANIZATION REPORT NUMBER
U.S. Army Research Laboratory ATTN: RDRL-SEE-E 2800 Powder Mill Road Adelphi, MD 20783-1197	ARL-TR-6419

9. SPONSORING/MONITORING AGENCY NAME(S) AND ADDRESS(ES)	10. SPONSOR/MONITOR'S ACRONYM(S)
	11. SPONSOR/MONITOR'S REPORT NUMBER(S)

12. DISTRIBUTION/AVAILABILITY STATEMENT

Approved for public release; distribution unlimited.

13. SUPPLEMENTARY NOTES

14. ABSTRACT

The development of a sensing platform to detect and identify biological, chemical, and energetic hazards is a long-sought-after goal of the Army and other first responder communities. Surface enhanced Raman scatting (SERS) is a spectroscopic technique gaining popularity as it address many sensing needs. However, despite the many advantages of SERS, it remains a marginalized sensing technique primarily due to the challenges in fabricating a reliable, highly sensitive, reproducible nanoscale surface. In this work, we demonstrate that many of the substrate fabrication challenges have been overcome by a newly developed, commercially available, next generation Klarite SERS substrate. These substrates are fabricated similarly to the standard Klarite substrates, but due to variations in the size and spacing of the surface features, they have increased sensing capabilities. The sensitivity for detecting the model SERS analyte, trans-1,2-bi-(4-pyridyl) ethylene (BPE) using both a 633- and 785-nm laser system is demonstrated. For one of the next generation substrates, the detection limit improved by as much as ~4 times for BPE (under some conditions). This improved performance may in part be attributed to physical changes to the substrate surface including an increased density of features and plasmon absorbance band locations.

15. Subject Terms

Raman, SERS, ammonium nitrate, Klarite

16. SECURITY CLASSIFICATION OF:			17. LIMITATION OF ABSTRACT	18. NUMBER OF PAGES	19a. NAME OF RESPONSIBLE PERSON
					Mikella E. Farrell
a. REPORT	b. ABSTRACT	c. THIS PAGE	UU	28	19b. TELEPHONE NUMBER *(Include area code)*
Unclassified	Unclassified	Unclassified			(301) 394-0948

Contents

List of Figures

List of Tables

Acknowledgments

INTENTIONALLY LEFT BLANK.

1. Introduction

The development and widespread use of sensing platforms for dynamic, real-time detection of hazardous materials (i.e., chemical, biological, and energetic) has remained a continuous goal in numerous fields of research, especially for the U.S. Army and other first responders. In order to rapidly detect and identify hazardous materials before or after exposure to human populations, such an ideal sensor must have the following characteristics:

- Operable in a host of different environments

- Sensitive to several types of target analytes at low concentrations

- Quantitative output

- Cost efficient

- Hand-held

- Requiring little to no sample preparation

- Commercially available.

To answer these needs, several sensing methodologies (for research and commercial use) have been proposed and developed. Some of the more common and effective hazard sensing technologies center on vibrational spectroscopy like Raman and related Raman-based techniques. Vibrational-based spectroscopic techniques like Raman rely on specific vibrations in a molecule from which a fingerprint spectrum can be generated for qualitative and quantitative measurements. Raman and Raman-based techniques are particularly well suited for the identifying and characterizing unknown targets, both hazardous and benign (*1–6*) as they (1) do not suffer from interferences from water, (2) require little to no sample preparation, (3) are robust and can be used in numerous environments, (4) are relatively insensitive to the wavelength of excitation employed, and (5) produce a narrowband spectral signature unique to the molecular vibrations of the analyte. All of these advantages contribute to Raman spectroscopy's capability to characterize, identify, and quantify samples. Despite such advantages, however, Raman spectroscopy has remained a somewhat marginalized technique for trace detection of hazardous materials in the field, mainly due to the extremely low scattering cross sections characteristic to many hazards.

Currently in the sensing community, one Raman-based technique—surface enhanced Raman scattering (SERS)—is gaining particular interest for hazard detection. SERS has all of the advantages of spontaneous Raman with the added benefit that electromagnetic and chemical enhancements contribute to increasing the overall signal. SERS is commonly observed when a molecule adsorbed onto or in close proximity to a nanoscale roughened metalized (typically gold

[Au] or silver [Ag]) surface has incident light directed onto it. This results in the excitation of the surface plasmons and thus greatly increasing the electromagnetic field of the light at the surface. Consequently, the Raman scattering of the molecule adsorbed on the surface is also amplified. The second contribution is due to a chemical effect and is assigned to the mixing of the orbitals of the adsorbed molecule and the metal atoms on the substrate surface. This second effect is considered much weaker (typically up to 2 orders of magnitude) than the electromagnetic effect. Under ideal conditions, SERS has been reported to detect single molecules (*7–9*). Compared to conventional Raman, the SERS enhancement has been reported to be as much as 14 orders of magnitude greater (under optimized conditions) (*9*), although it is most commonly observed to be 6 to 8 orders of magnitude. SERS has already been shown to be a viable sensing technique for chemical, biological, and energetic hazard detection in laboratory settings (*6, 10–15*). Thus, with continued efforts towards fabricating a more dynamic sensitive sensor, SERS has the potential to serve as a universal rapid screening tool for many types of hazardous materials.

Despite its many advantages, the application of SERS to real-world situations has remained challenging due in part to the difficulty of fabricating highly sensitive and spectrally/physically reproducible SERS substrates (*16–18*). Several SERS platforms have been fabricated and demonstrated in the literature including colloids (*19*), film over nanospheres (*20–23*), fiber optic bundles (*1*), nanoparticles (*24–28*), and lithographically (*29*) produced structures. At best, the more sensitive substrate platforms have a 15% relative standard deviation (RSD), the measure of the reproducibility of an analysis, from substrate-to-substrate and a SERS signal enhancement of 7 to 8 orders of magnitude (*21, 22*). Consequently, many researchers in academia, industry, and government have focused concerted efforts toward increasing the enhancement ability, reproducibility, and mass production manufacturing of substrates to increase the utility of this technique (*29, 30*). For the Army and first responders, such a substrate platform with increased sensitivity and reliability would be very advantageous for detecting and identifying unknowns.

Research efforts have also concentrated on better directing the optimization of the substrate surface from which the SERS enhancement occurs (*17, 29, 31–33*). Based in part on experimental and theoretical efforts, the directed fabrication of SERS platforms has focused on modifying the feature size (*34–36*), spacing between objects, geometry and shape of structures (*37–39*), identity and incorporation of metals on the surface (*40*), feature height, and the character of the foundation layer (*3, 14, 20, 41*) and the architecture on which it is fabricated (*11, 42, 43*). Numerous examples in the literature detail how varying some of these parameters, in some cases, can result in very dramatic changes to the overall SERS enhancing capabilities of the substrate surface. Rigorous efforts continue to focus on understanding how these parameters, as well as a vast number of others, synergistically work together to result in a highly reproducible sensitive SERS substrate. As the overall sensing capabilities of the SERS surface improves, congruent research is pushing toward developing the uniform, reproducible, mass producible platform needed to facilitate widespread adoption of SERS as a viable sensing technology.

Some success fabricating both spectrally and physically reproducible SERS substrates has been demonstrated with commercially available standard Klarite™ substrates (Renishaw Diagnostics) (*32, 44–47*). These substrates were developed using a well-defined silicon-based semiconductor fabrication technique in which a silicon diode mask is defined by optical lithography and then surface etched using potassium hydroxide (KOH), resulting in an array of highly reproducible inverted pyramid features (*47*). These array pyramids are reported to have "hot spots" or "trapped plasmons" located inside the wells (*47*). These substrates have been previously characterized (*48*) using atomic form microscopy (AFM) images, which showed that the inverted pyramids were about 1.47 μm wide and 1 μm deep. These substrates have plasmon absorbance bands located at 577 and 749 nm, thus demonstrating the usefulness of this substrate for a range of excitation sources. In addition, due to the fabrication process used, under ideal conditions, these substrates have demonstrated typical RSDs ranging from 10%–15% under drop and dry conditions.

While these standard Klarite substrates do demonstrate a high degree of substrate reproducibility and very low substrate background interference (SERS signal and surface morphology), for many applications in real-world situations, increased analyte sensitivity is still necessary. Recently, new prototype Klarite based substrates have been fabricated by Renishaw Diagnostics with the intent to expand substrate sensing capabilities. The morphologies of these substrates dramatically differ in overall shape, pitch, and spacing as compared to the standard Klarite substrate resulting in very interesting sensing capabilities.

In this report, we report on the physical characterization of these substrates to include AFM, scanning electron microscopy (SEM), and plasmon absorbance data. We also discuss the reproducibility and limit of detection results as determined with the next generation Klarite SERS substrates using a model compound, trans-1,2-bi-(4-pyridyl) ethylene (BPE) measured at two different wavelengths 633 and 785 nm in a Renishaw Raman Microscope.

2. Experimental

2.1 Commercially Available Substrates

Commercially available, slide-mounted standard Klarite 302 SERS substrates were purchased from Renishaw Diagnostics. Slides were received individually wrapped and vacuum sealed. The SERS active area on these slides is a gold-coated 4 mm x 4 mm wafer. The standard Klarite slides were only used once and opened just prior to measurement to reduce any possible surface fouling. In addition, the substrate was submerged in ethanol prior to initial measurements to remove any possible contamination that may have accumulated on the surface. Next generation Klarite substrates (designated as 308's and 309's) were used as received from Renishaw Diagnostics following the same procedures used for the standard substrates. Due to a limited

number of substrates available, data were collected using a standard addition method. Typically, in SERS data collection on the standard and 308 substrates, five measurements across the substrate surface were collected. The next generation 309 substrate is composed of four distinct quadrants, and due to the limited active surface area on the 309's, only two measurements were collected per quadrant. Most data in this report are presented as an average of a collected data set and one standard deviation error shown, unless otherwise indicated.

2.2 Instrumentation and Data Analysis

Plasmon data were obtained using an Avantes system. The system is controlled using AvantesSpec software. Data analysis was performed using Igor Pro 4.0 (WaveMetrics, Inc.). Unless otherwise indicated, data acquisition parameters were 500-ms exposure time for 10 accumulations and 3 averages. Using this methodology a total of five spectra were collected from each substrate. SEM images was obtained using a FEI environmental SEM (Quanta 200 FEG). A Renishaw in Via Reflex Raman microscope was used for SERS and Raman spectra collection. Spectra were collected using the near-infrared (NIR) 785-nm laser. The laser light was focused onto the sample using a 5× objective, exposures were 10 s long, and three accumulations were collected per spot. Approximately 7 mW of power irradiated the surface of the substrate. Samples were positioned using a motorized XYZ translational stage internal to the microscope. Spectra were collected, and the instrument was run using Wire 3.2 software operating on a dedicated computer. Data analysis was achieved using IgorPro 6.0 software (Wavemetrics) (*10*). All AFM data were obtained using a Veeco AFM. The AFM was operated in tapping mode using two tips, the OTESPA Veeco (frequency 300 kHz, length 110–180 μm), and the TAP 150Al-G Budget Sensor (soft tapping mode, resonant frequency 150 KHz).

2.3 Chemicals and Reagents

All chemicals were used as received without further purification. For the evaluation of substrate sensing capabilities, the SERS active chemical BPE in ethanol (EtOH) was used. The analyte BPE was used as it is a well characterized SERS active compound (all bands assigned), binds to Ag and Au, and does not resonantly enhance in the visible (*49*). The SERS response test protocol used a modified standard addition methodology developed (in partnership with Edgewood Chemical Biological Center) and commonly used for SERS Defense Advanced Research Projects Agency (DARPA) evaluation program (*6, 10, 33, 43, 50, 51*). Briefly, in these experiments the substrate was soaked in 5 mL of a BPE/EtOH solution for 10 min to insure complete binding of the BPE with the surface, and then the SERS spectra of the substrate were collected from five different points across the substrate (while still in solution). Once the measurements were collected, the old solution was removed and the substrate was soaked in the next concentration of BPE/EtOH solution. Following this protocol, typical BPE solution concentration additions included blank none, EtOH, 1×10^{-14}, 1×10^{-13}, 1×10^{-12}, 1×10^{-11}, 1×10^{-10}, 5×10^{-10}, 1×10^{-09}, 5×10^{-09}, 7.5×10^{-09}, 1×10^{-08}, 2.5×10^{-08}, 5×10^{-08}, 7.5×10^{-08}, 1×10^{-07}, 2.5×10^{-07}, 5×10^{-07}, 7.5×10^{-07}, and 1×10^{-06} M BPE, for a total of 20 measurements.

2.4 Data Analysis

For evaluation of substrate SERS enhancing capabilities, the intensity of the 1200 cm^{-1} SERS ethylenic C=C stretch band of BPE was used to quantify the signal-to-noise (S/N) ratio due to its reasonable insensitivity to orientation on the surface (*52*). In figure 1, a typical SERS spectrum of BPE is shown, relevant vibrations are identified.
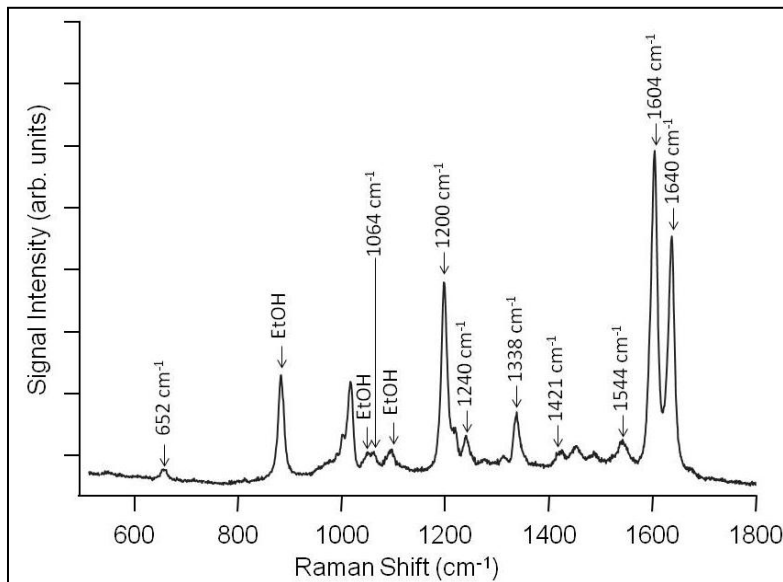
Figure 1. Example SERS spectrum of the analyte BPE immersed in EtOH.
Relevant bands are clearly called out. For data analysis purposes,
the 1200 cm^{-1} band of BPE was used.

2.5 Calculations

Sample calculations are shown in table 1. In this table the physical parameters measured on the substrates and those calculated are defined. The S/N ratio is defined as

$$\text{S/N Ratio} = \frac{(\text{Signal at 1200 cm} - 1 \text{ band}) - (\text{Average Signal of Baseline })}{(\text{standard deviation of baseline})} \tag{1}$$

5

Table 1. Sample calculations and physical parameters measured.

Assignment	Equations	Explanation
A	measured	length base (nm)
B	measured	width base (nm)
C	= A x B	Base Area (m^2)
D	= 2(A+B)	Perimeter (nm)
E	= (1/2)A	half leg (nm)
F	measured	altitude (nm)
G	= ((D^2) + (F^2))^0.5	Slant length (nm)
H	= (1/2) A x G	area one side (triangle) (nm^2)
I	= 4(H) + C	area 4 sides+base (nm^2)
J	= 4(H)	area 4 sides (nm^2)
K	measured	Length one feature base + (1/2 distance between features)
L	= K^2	area feature base + (1/2 distance between features)
M	= (1-C/L) x 100	% "NonActive" in total base area
N	measured	active area (m^2) chip= 4x4, quadrant 1.92 x 1.92
O	= K x (1 x 10^-9)	base area per entire feature (mm^2)
P	= N/O	Density = number of features/ active area

3. Results and Discussion

An "ideal standard" SERS sensor would demonstrate many advantages including (1) analyte sensitivity and (2) morphological and spectral uniformity. Working towards the goal of fabricating a more universal SERS sensing platform, widespread research efforts have concentrated on modifying the physical components of the substrate architecture. Physical factors that can be modified for a dramatic overall impact to the SERS substrate sensing capabilities include changing the size, shape, and spacing between structural features as well as modifying the dielectric environment. The experimental literature has multiple examples demonstrating that the largest overall SERS signal enhancement occur when the substrate surface is composed of nanoscale features (characterized in a multitude of effective and sometimes different geometries) in close proximity to each other, and that at or near the junctions of these nanofeatures is where the largest overall field enhancement or hotspots appear (*22, 34, 53*).

Given that modifying the SERS substrate architecture can dramatically change the overall SERS signal enhancing capabilities of the substrate, we have evaluated many SERS substrates (commercial and academic) following a procedure developed for the DARPA SERS Fundamentals program. Examples of SERS substrates tested from a commercial source include Q-SERS, standard Klarite SERS substrates, and next generation Klarite SERS substrates. The

next generation substrates are based on the commercially available standard Klarite substrate, with modifications to the size and spacing of features. Evaluation of these substrates for future potential Army applications was performed by documenting their physical properties and sensing capabilities with a commonly used SERS active analyte BPE. The preliminary characterization results from the U.S. Army Research Laboratory analyzed next generation Klarite prototypes follow.

Standard and next generation Klarite substrates were physically characterized by SEM image analysis and AFM, which is necessary to better understand the morphological changes between the two and draw conclusions from possible trending. SEM analysis provides insight into the spacing and size of substrate features, while AFM data analysis provides topographical information to accurately determine the exact feature size and depth. Combining data from these two techniques creates an in-depth analysis of overall substrate morphology from which we can estimate the "active" substrate surface area, determine the degree of pitch, and identify any trends.

In figure 2, the combined SEM and AFM data are shown in a visual schematic of the standard and next generation Klarite substrates. Example physical parameters are measured with AFM: the sensing area for the different substrates and an example SEM image are displayed. In figure 2a, a schematic graphic of a typical Klarite substrate is demonstrated with the Klarite chip's active area shown. Substrates can be purchased mounted onto a standard glass microscope slide or unmounted. Figure 2b includes a description of AFM data for a substrate with inverted pyramids clearly shown: (A) is the length of a pyramid, (B) is the height of a pyramid, (C) is the spacing between the inverted pyramids, and (D) is the length of the pyramid wall. In figure 2c, the sensing area for the three different types of substrate is shown. Klarite 302 and 308 are both composed of a single uniform sensing area that measures approximately 4 mm by 4 mm, while Klarite 309 consists of four different sensing quadrants each measuring approximately 1.92 mm by 1.92 mm. In figure 2d, a modified SEM image demonstrates the different areas on the substrate measured. This image includes an inner (active, in black marks) and outer (overall area, in white marks) portion of an inverted pyramid marked: (a) length of pyramid and (c) spacing between pyramids. It should be noted that the spacing between the features, the depths of the features, and in some cases, the number of overall features differed from substrate to substrate type. All of these measurements are used for estimating the standard sensing area per inverted pyramid (calculation accounts for pyramid structure) and the overall percentage of active sensing area per chip; see section 2 for more details. From this analysis, conclusions and explanations for possible trending can be drawn.
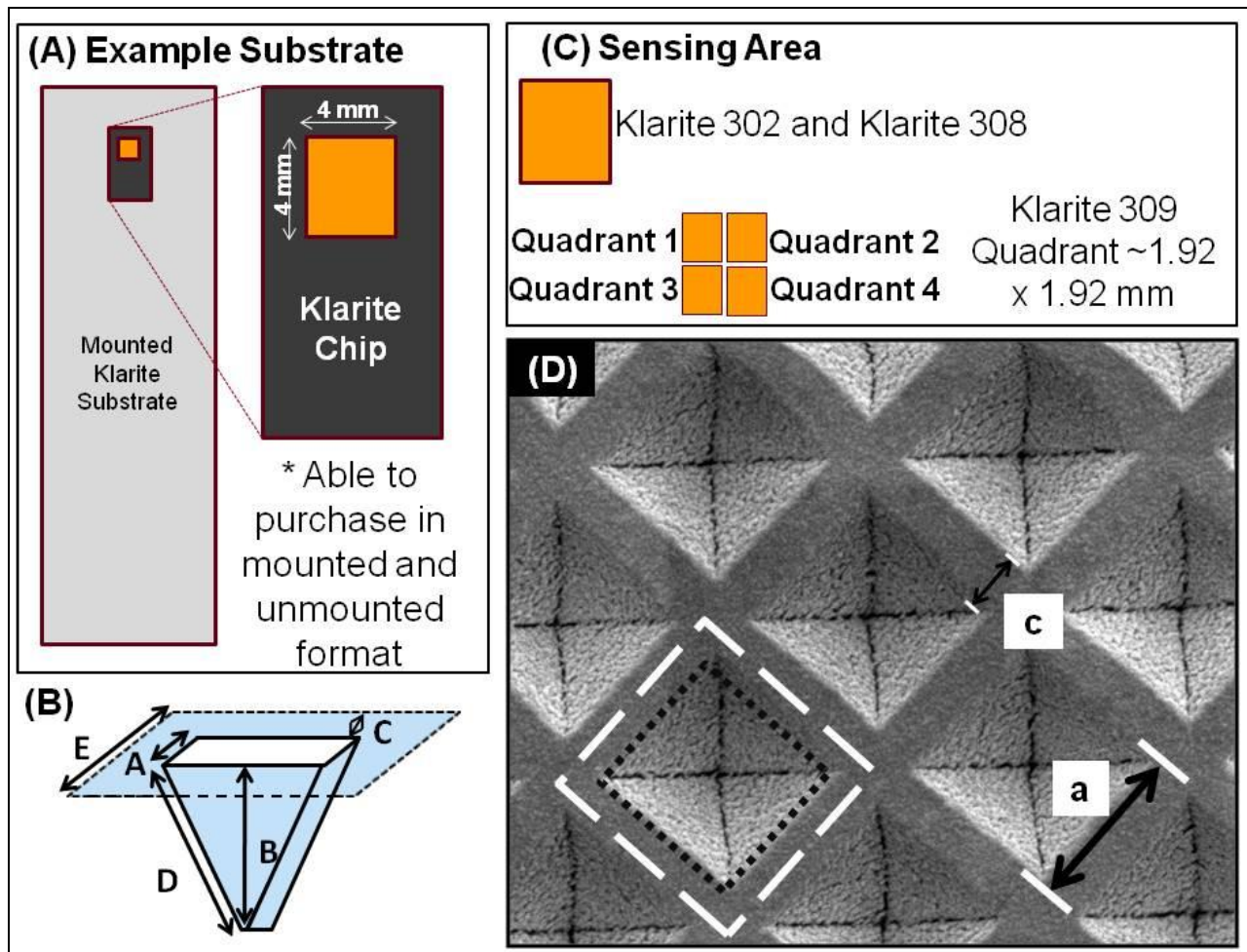
Figure 2. A visual schematic of standard and next generation Klarite substrates is shown. (a) A drawing of a typical Klarite substrate with the Klarite chip, demonstrated for clarity. (b) AFM data for the substrate with inverted pyramids: (A) is the length of a pyramid, (B) is the height of a pyramid, (C) is the spacing between the inverted pyramids, (D) is the length of the pyramid wall, and (E) is the overall feature size. (c) The sensing area for the three different types of substrate, showing that Klarite 302 and 308 are both composed of a single uniform sensing area, while Klarite 309 consists of four different quadrants. (d) A modified SEM image showing the different measurements on the substrate, inner (active, in black marks) and outer (overall area, in white marks) portion of an inverted pyramid: (a) length of pyramid and (c) spacing between pyramids.

To establish the total number of cells (inverted pyramids + ½ the distance between the neighbor cell) for the active area of the substrate and determine the total % of the surface that was composed of cells, a combination of information from both SEM and AFM analysis was employed. Using SEM and AFM data analysis sizes of inverted pyramids for the different types of Klarite substrate were established; figure 3a shows an example SEM of a Klarite 309 substrate and figure 2b shows the same for the AFM data. From data analysis, we determined that a standard Klarite substrate has an outer width of about 2040 nm and an inner pyramid width of 1470 nm, for a total sensing area of 51.9% of a single pyramid. Assuming an overall active chip size of 4 mm x 4 mm, the total number of cells for each 302 substrate is around 3.84×10^6. The

Klarite 308 substrate has an outer width of 636.4 nm, and an inner pyramid width of about 454.0 nm, for a total sensing area of 50.9% of a single pyramid. Assuming an overall active chip size of 4 mm x 4 mm, the total number of cells for each 308 substrate is around 3.95 x 10^7. Similar calculations were conducted for the different quadrants of Klarite 309 (table 2). From this information, we conclude that the next generation Klarite 308 has a significantly higher overall density of cells for the surface area as compared to the Klarite 302, and thus, potentially a greater increased number of SERS hot spots. Ranking the percentage of cell "active" greatest to smallest on the 309 substrate quadrant, 3 is largest, followed by quadrant 1, followed by quadrant 4, and then quadrant 2, which has the smallest overall percentage of active area. From this observed trending on the 309 substrate, we could conclude that quadrant 3 will outperform quadrant 2.
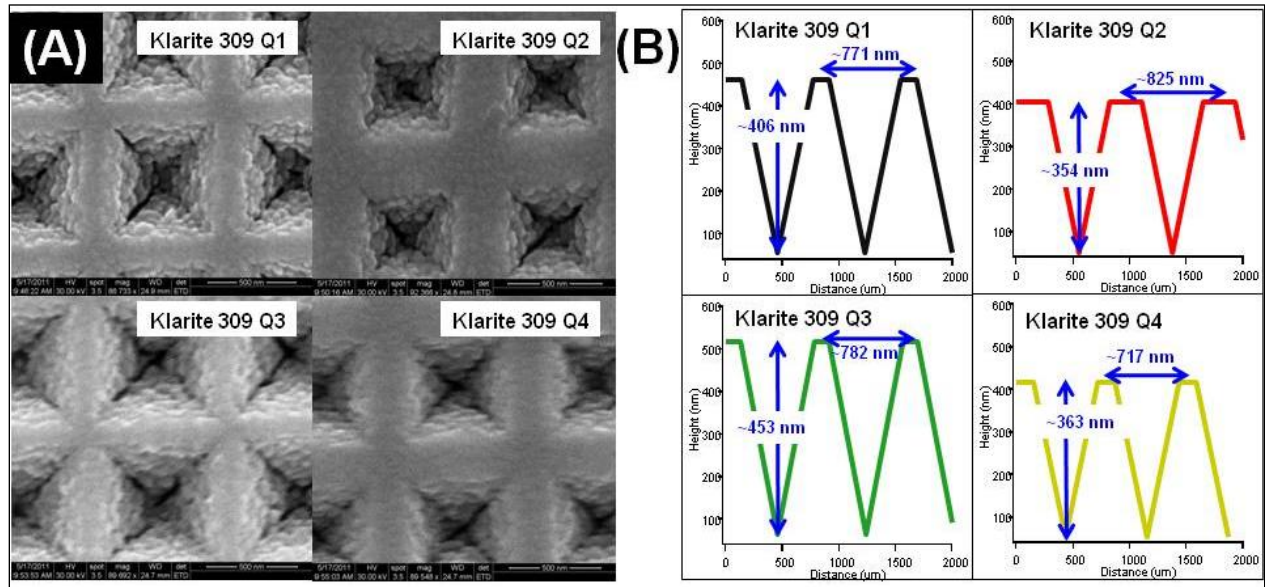

Figure 3. (a) SEM images of different quadrants of Klarite 309 substrate and (b) typical approximate AFM data collected from each of the four quadrants of Klarite 309. From this data, quadrant 1 has a depth of about 406 nm, quadrant 2 has a depth of about 354 nm, quadrant 3 has a depth of about 453 nm, and quadrant 4 has a depth of about 363 nm.

Table 2. Comparison physical parameters of standard Klarite, Klarite 308, and Klarite 309 quadrants as determined by SEM and AFM analysis.

Substrate Type	Total number of cells for chip area	(a) Well width (nm)	(b) Height well (nm)	(c) Distance between features (nm)	(d) Slant length	Pyramid surface area	% of "cell" area active
Klarite 302	3.84E+06	1470	1000	570	1428	2.43E+13	51.9%
Klarite 308	3.95E+07	454	278	200	422	2.17E+11	50.9%
Klarite 309 Q1	6.41E+06	630	406	141	514	2.57E+11	66.7%
Klarite 309 Q2	5.67E+06	543	354	282	446	1.43E+11	43.3%
Klarite 309 Q3	5.90E+06	652	453	130	558	3.09E+11	69.5%
Klarite 309 Q4	5.67E+06	565	363	152	460	1.66E+11	62.0%

To get an overall idea about the depths of features across the surface and overall pyramid surface area, AFM analysis was used. In table 1, a summary of these results is provided including the number of cells per chip area, well width and height, distance between features, slant length, pyramid surface area, and percentage of cell area deemed active for the standard commercial Klarite 302 and the prototype Klarite 308 and 309 series. Comparing the pyramid surface area between the 302 and the 308, we see that overall the 302 has a much larger surface area. However, there are significantly more "cells" for the Klarite 308 as compared to 302, and the cells are placed much more closely together, which might affect overall SERS signal enhancing capabilities. The trend observed from largest to smallest overall inverted pyramid surface area and active area on the Klarite 309 is quadrant 3, quadrant 1, quadrant 4, and quadrant 2. Additionally when comparing the different quadrants of the 309, it can be observed that ranking pyramid depth (B) from greatest to smallest we observe the following trend: quadrant 3, quadrant 1, quadrant 4, and quadrant 2. Comparing spacing between features smallest to greatest, we again observe the trend going from quadrant 3, quadrant 1, quadrant 4, and finally quadrant 2. All of these physical parameters may have a significant influence on the overall SERS activity of these different quadrants.

It has been demonstrated in the literature that the overall maximum SERS signal enhancement occurs when the localized surface plasmon resonance (LSPR) falls between the wavelength of excitation and the Stokes frequency shift (*54–56*). As the SERS intensity is dependent upon the excitation of the LSPR, it is important to better optimize the experimental setup to evaluate these substrates. Therefore, the plasmon absorbance data for the different SERS substrates were collected (figure 4). The plasmon absorbance band for the standard Klarite was previously

reported to be located at 577 and 749 nm. The plasmon absorbance band for Klarite 308 is located at 590 and 675 nm, the Klarite 309 quadrant 1 plasmon bands are located at 723 and 840 nm, quadrant 2 is located at 700 and 831 nm, quadrant 3 is located at 734 and 845 nm, and quadrant 4 is located at 713 and 836 nm. The plasmon bands of Klarite 302 and 308 are found to be most similar in location. The location of the second plasmon band feature for the different quadrants of 309 ranked from greatest to lowest wavelength are: quadrant 3, quadrant 1, quadrant 4, and quadrant 2.
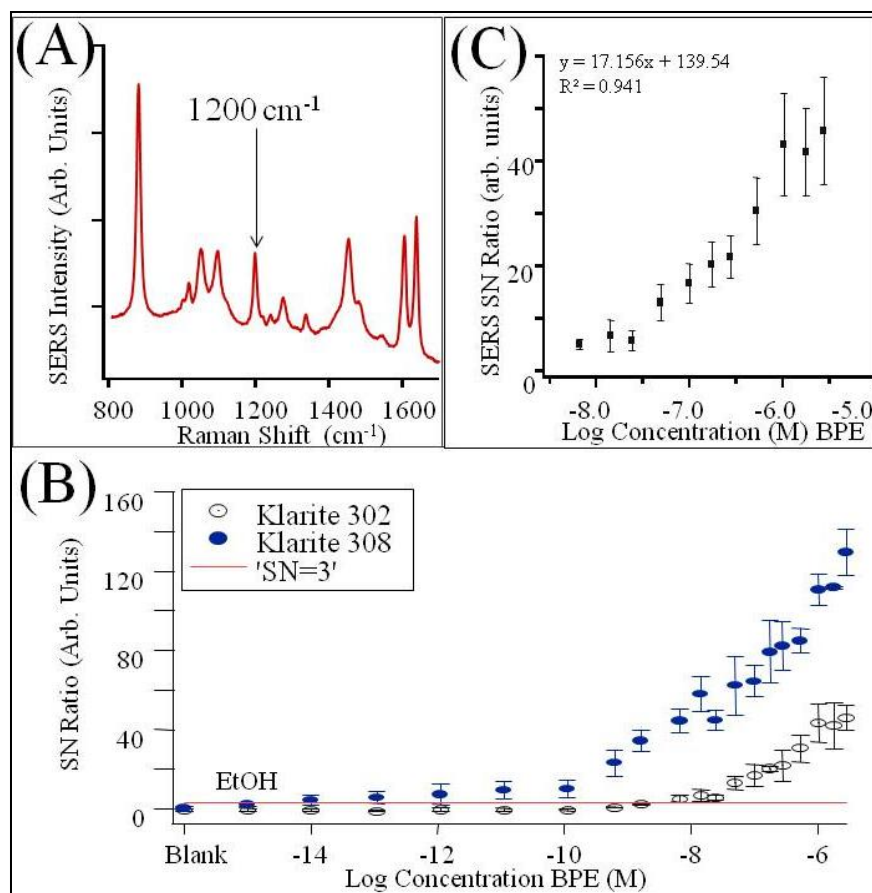
Figure 4. (a) Typical BPE spectrum shown with 1200 cm^{-1} band indicated. (b) Comparison of S/N ratio of Klarite 308 and 302. Red line indicates S/N=3. (c) Example of results from a standard Klarite substrate, collected with 785 nm laser, averaged data points with S/N >3, error represents 1 std. dev. In this data set, the R^2 value observed is 0.941. Quadrant 3 (Q3) is shown to have the overall highest SERS sensing capabilities.

Limits of detection (LOD) and overall typical S/N ratios were determined following the SERS BPE testing evaluation previously described and briefly outlined in section 2. For these experiments, two different wavelengths were evaluated to determine if the location of the plasmon band would influence the overall SERS response of the substrates. For LOD determination, the S/N ratios and error were calculated for all substrate types over 20 different calculations and at two different wavelengths. The target analyte used was BPE (see figure 3a for

an example spectrum of BPE at 785 nm in EtOH) with the 1200 cm^{-1} band clearly indicated. In figure 3b, an example S/N comparison between the Klarite 302 and 308 is clearly demonstrated. An example of data analysis is shown in figure 3c from a standard Klarite substrate, collected with a 785-nm laser, showing the averaged data points with a S/N >3 and the error represents 1 std. dev. In this data set, the R^2 value observed is 0.941. Using this type of analysis, it was possible to calculate the sensitivity for all substrate types at the two different wavelengths (see table 2 for a summary of results). It should be noted that this LOD is analyte specific, as different chemical interactions between the surface and the analyte can occur by changing the identity of the chemical of interest. Similar data were collected and analyzed for both the 633- and 785-nm laser (see table 2 for a summary of LOD results).

The results shown in table 3 clearly show that the best results were obtained using Klarite 308 with 785-nm excitation, yielding an overall improvement of almost 4 orders of magnitude greater in LOD for this analyte compared to the standard Klarite 302 under the same experimental conditions. Using 633-nm laser excitation, the data show that the Klarite 308 outperforms other substrates; however, the changes in sensing capabilities were not substantial. From the characterization data discussed (density comparison, amount of active area, location of plasmon absorbance bands) previously, some trending correlates with overall SERS sensing performance observed. This implies that there might be other parameters besides those measured affecting overall SERS enhancing capabilities.

Table 3. Comparison of standard Klarite 302, Klarite 308, and Klarite 309 quadrants as determined by SEM analysis and limits of detection determination at 633 nm and 785 nm.

Substrate Type	Plasmon Location	(Number of Cells) X (Surface Area)	LOD at 633-nm laser excitation (BPE)	LOD at 785-nm laser excitation (BPE)
Klarite 302	577, 749	9.32E+19	5.83E–09	1.99E–08
Klarite 308	590, 675	8.60E+18	6.27E–10	9.46E–13
Klarite 309 Q1	723, 840	1.59E+18	1.98E–09	5.40E–08
Klarite 309 Q2	700, 831	7.74E+17	2.88E–08	1.99E–08
Klarite 309 Q3	734, 845	1.87E+18	2.16E–09	6.89E–09
Klarite 309 Q4	713, 836	1.19E+18	1.97E–09	2.31E–08

4. Conclusions

In this report, we characterized and compared next generation Klarite substrates 308 and 309 to the standard Klarite substrate at different excitation wavelengths, 633 and 785 nm. From the characterization results, we showed that the next generation Klarite substrate's SERS sensing performance is significantly better (up to 4 orders of magnitude, in some cases) as compared to the standard Klarite 302. Future work will focus on testing next generation Klarite response to various energetic samples and modeling efforts to determine hot spot location across a substrate surface. In addition, as these substrates are optimized and made more market ready, we expect to re-evaluate their sensitivity and reproducibility.

5.   References

1.   Hankus, M. E.; Cullum, B. M. SERS Probes for the Detection and Imaging of Biochemical Species on the Nanoscale. *Proceedings of the SPIE - The International Society for Optical Engineering*, 2006, p. 638004-1–12.

2.   Hankus, M. E.; Cullum, B. M. SERS Nanoimaging Probes for Characterizing Extracelllar Surfaces - Art. no. 675908. *Smart Biomedical and Physiological Sensor Technology V* **2007**, *6759*, 75908–75908.

3.   Hankus, M. E., et al. Surface-enhanced Raman Scattering (SERS) - Nanoimaging Probes for Biological Snalysis. *Smart Medical and Biomedical Sensor Technology Ii* **2004**, *5588*, 106–116.

4.   Hankus, M. E.; Gibson, G. J.; Cullum, B. M. Characterization and Optimization of Novel Surface-enhanced Raman Scattering (SERS)-based NanoImaging Probes for Chemical Imaging. *Proceedings of the SPIE - The International Society for Optical Engineering*, 2005, p. 600704-1–11.

5.   Hankus, M. E., et al. Surface-enhanced Raman Scattering-based Nanoprobe for High-Resolution, Non-scanning Chemical Imaging. *Analytical Chemistry* **2006,** *78* (21), 7535–7546.

6.   Hankus, M. E.; Stratis-Cullum, D. N.; Pellegrino, P. M. *Towards Advanced Biological Detection Using Surface Enhanced Raman Scattering (SERS)-based Sensors.* Biosensing Iii, 2010, **7759**.

7.   Kneipp, K.; Kneipp, H. Detection, Identification, and Tracking of Biomolecules at the Single Molecule Level using SERS. *Biophysical Society* **2005**.

8.   Kneipp, K.; Kneipp, H. Single Molecule Raman Scattering. *Appl. Spectros.* **2006**, *60*, 322A.

9.   Kneipp, K., et al. Single Molecule Raman Spectroscopy Using Silver and Gold Nanoparticles. *Indian Journal of Physics and Proceedings of the Indian Association for the Cultivation of Science-Part B* **2003**, *77B* (1), 39–47.

10.   Hankus, M .E.; Stratis-Cullum, D. N.; Pellegrino, P. M. Characterization of Next-generation Commercial Surface-enhanced Raman Scattering (SERS) Substrates. *Proc. SPIE* **2011**, *8018*, 80180P.

11.   Holthoff, E. L.; Stratis-Cullum, D. N.; Hankus, M. E. Xerogel-Based Molecularly Imprinted Polymers for Explosives Detection. *Chemical, Biological, Radiological, Nuclear, and Explosives (Cbrne) Sensing Xi* **2010**, 7665.

12. Holthoff, E. L.; Stratis-Cullum, D. N.; Hankus, M. E. A Nanosensor for TNT Detection Based on Molecularly Imprinted Polymers and Surface Enhanced Raman Scattering. *Sensors* **2011**, *11* (3), 2700–2714.

13. Holthoff, E. L., et al. ANYL 57-Nanosensor for Explosives' Detection Based on Molecularly Imprinted Polymers and Surface Enhanced Raman Scattering. *Abstracts of Papers of the American Chemical Society* **2009**, *238*, 57–ANYL.

14. Jian, S.; Hankus, M. E.; Cullum, B. M. SERS Based Immuno-microwell Arrays for Multiplexed Detection of Foodborne Pathogenic Bacteria. *Proceedings of the SPIE - The International Society for Optical Engineering* **2009**, 73130K (10 pp).

15. Guicheteau, J., et al. Bacillus Spore Classification via Surface-Enhanced Raman Spectroscopy and Principle Component Analysis. *Applied Spectroscopy* **2008**, *62* (3), 267–272.

16. Homola, J.; Yee, S. S.; Gauglitz, G. Surface Plasmon Resonance Sensors: Review. *Sensors and Actuators B-Chemical* **1999**, *54* (1–2), 3–15.

17. Kneipp, K., et al. Surface-enhanced Raman Scattering: A New Tool for Biomedical Spectroscopy. *Current Science* **1999**, *77* (7), 915–924.

18. Kneipp, K., et al. Ultrasensitive Chemical Analysis by Raman Spectroscopy. *Chemical Reviews* **1999**, *99* (10), 2957–+.

19. Qian, X. M., et al. In Vivo Tumor Targeting and Spectroscopic Detection with Surface-Enhanced Raman Nanoparticle Tags. *Nature Biotechnology* **2008**, *26* (1), 83–90.

20. Li, H.; Baum, C. E.; Cullum, B. M. Characterization of Novel Gold SERS Substrates with Multilayer Enhancements. *SPIE* **2006**, 6380.

21. Li, H., et al. Multilayer Enhanced SERS Active Materials: Fabrication, Characterization, and Application to Trace Chemical Detection. *SPIE* **2006**, *6218*, 621804.

22. Li, H.; Patel, P. H.; Cullum, B. M. Novel Multilayered SERS Substrates for Trace Chemical and Biochemical Analysis. *SPIE* **2004**, *5588*.

23. Vo-Dinh, T., Cullum, B. M.; Stokes, D. L. Stokes. *Nanosensors and Biochips: Frontiers in Biomolecular Diagnostics*. 2001: Elsevier Science Sa.

24. Cao, Y.W.C.; Jin, R. C.; Mirkin, C. A. Nanoparticles with Raman Spectroscopic Fingerprints for DNA and RNA Detection. *Science* **2002**, *297*, 1536.

25. Chowdhury, M. H., et al. Use of Surface-enhanced Raman Spectroscopy for the Detection of Human Integrins. *Journal of Biomedical Optics* **2006**, *11* (2), 8.

26. Culha, M., et al. Characterization of Thermophilic Bacteria Using Surface-Enhanced Raman Scattering. *Applied Spectroscopy* **2008**, *62* (11), 1226–1232.

27. Jarvis, R. M., et al. Surface-Enhanced Raman Scattering from Intracellular and Extracellular Bacterial Locations. *Analytical Chemistry*, **2008**, *80* (17), 6741–6746.

28. Kneipp, J.; Kneipp, H.; Kneipp, K. SERS - A Single-molecule and Nanoscale Tool for Bioanalytics. *Chemical Society Reviews* **2008**, *37* (5), 1052–1060.

29. Tripp, R. A.; Dluhy, R. A., Zhao, P.*el* Nanostructures for SERS Biosensing. *Nano Today* **200**, *3* (3–4), 31–37.

30. Driskell, J. D., et al. Infectious Agent Detection with SERS-active Silver Nanorod Arrays Prepared by Oblique Angle Deposition. *IEEE Sensors Journal* **2008**, *8* (5–6), 863–870.

31. Norrod, K. L., et al. Quantitative Comparison of Five SERS Substrates: Sensitivity and Limit of Detection. *Appl. Spectros.* **1997**, *51* (7), 994.

32. Alexander, T. A.; Le, D. M. Characterization of a Commercialized SERS-active Substrate and its Application to the Identification of Intact Bacillus Endospores. *Appl. Opt.* **2007**, *46* (18).

33. Guicheteau, J., et al. Assessing Metal Nanofabricated Substrates for Surface-Enhanced Raman Scattering (SERS) Activity and Reproducibility. *Applied Spectroscopy* **2011**, *65* (2), 144–151.

34. Jones, J. P., et al. Photonic Nanostructures as SERS Substrates for Reproducible Characterization of Bacterial Spores. *SPIE* **2004**, *5416*, 94–104.

35. Kneipp, H., Kneipp, K. Surface-enhanced Hyper Raman Scattering in Silver Colloidal Solutions. *Journal of Raman Spectroscopy* **2005**, *36* (6–7), 551–554.

36. Kao, P., et al. Surface-enhanced Raman Detection on Metalized Nanostructured Poly(p-xylylene) Films. *Advanced Materials* **2008**, *20* (18), 3562–+.

37. Becker, M., et al. Nanowires Enabling Sgnal-enhanced Nanoscale Raman Spectroscopy. *Small* **2008**, *4* (4), 398–404.

38. Xie, J., et al. The Synthesis of SERS-Active Gold Nanoflower Tags for In Vivo Applications. *ACS Nano* **2008**, *2* (12), 2473–2480.

39. Braun, G., et al. Chemically Patterned Microspheres for Controlled Nanoparticle Assembly in the Construction of SERS Hot spots. *J. Am. Chem. Soc.* **2007**, *129*, 7760–7761.

40. Kho, K. W., et al. Deposition Method for Preparing SERS-Active Gold Nanoparticle Substrates. *Analytical Chemistry* **2005**, *77* (22), 7462–7471.

41. Kuncicky, D. M.; Prevo, B. G.; Velov, O. D. Controlled Assembly of SERS Substrates Templayed by Colloidal Crystal Films. *J. Mater. Chem.* **2006**, *16*, 1207–1211.

42. Kneipp, K.; Kneipp, H.; Kneipp, J. Surface-enhanced Raman Scattering in Local Optical Fields of Silver and Gold Nanoaggregatess - From Single-molecule Raman Spectroscopy to Ultrasensitive Probing in Live Cells. *Accounts of Chemical Research* **2006**, *39* (7), 443–450.

43. Lee, C. H., et al. Highly Sensitive SERS Substrates Based on Filter Paper Loaded with Plasmonic Nanostructures. *Anal. Chem* **2011**, Nov 3. [Epub ahead of print].

44. Alexander, T. A. Applications of Surface-Enhanced Raman Spectroscopy (SERS) for Biosensing: An Analysis of Reproducible, Commercially Available Substrates. *SPIE* **2005**, *6007*, 600703.

45. Alexander, T. A. Development of Methodology Based on Commercialized SERS-active Susbtrates for Rapid Discrimination of Poxviridae Virions. *Anal. Chem.* **2008**, *80* (8), 2817–2825.

46. Alexander, T. A.; Pellegrino, P. M.; Gillespie, J. B. Near-infrared Surface-Enhanced-Raman-Scattering-Mediated Detection of Single Optically Trapped Bacterial Spores. *Applied Spectroscopy* **2003**, *57* (11), 1340–1345.

47. Netti, M. C., et al. Probing Molecules by Surface-enhanced Raman Spectroscopy. *SPIE* **2006**, *6093.*

48. Hankus, M.; Stratis-Cullum, D.; Pellegrino, P. *Enabling Technologies for Point and Remote Sensing of Chemical and Biological Agents Using Surface Enhanced Raman Scattering (SERS) Techniques;* A; ARL-TR-4957; U.S. Army Research Labortory: Adelphi, MD, 2009.

49. Van Duyne, R.P., J.C. Hulteen, and D.A. Treichel, J. Chem. Phys., 1993. **99**: p. 2101.

50. Guicheteau, J., et al. Raman and Surface-enhanced Raman for Military Applications. *AIP Conference Proceedings*, 2010, 1267.

51. Hankus, M. E.; Stratis-Cullum, D. N.; Pellegrino, P. M. Surface Enhanced Raman Scattering (SERS)-based Next Generation Commercially Available Substrate: Physical Characterization and Biological Application. *Proceedings of the SPIE - The International Society for Optical Engineering*, 2011, 8099.

52. Yang, W.H., et al. A Surface-enhanced Hyper-Raman and Surface-enhanced Raman Scattering Study of Trans-1,2-bis(4-pyridyl)ethylene adsorbed onto Silver Film Over Nanosphere Electrodes. Vibrational Assignments: Experiment and Theory. *J. Phys. Chem.* **1996**, *104*, 4313–4323.

53. Tripp, R. A.; Dluhy, R. A.; Zhao, Y. Novel Nanostructures for SERS Biosensing. *Nano Today* **2008**, *3* (3–4), 31-37.

54. Albella, P., et al. Shape Matters: Plasmonic Nanoparticle Shape Enhances Interaction with Dielectric Substrate. *Nano Letters* **2011**, *11* (9), 3531–3537.

55. Henry, A.-I., et al. Correlated Structure and Optical Property Studies of Plasmonic Nanoparticles. *Journal of Physical Chemistry C* **2011**, *115* (19), 9291–9305.

56. Blaber, M. G., et al. LSPR Imaging of Silver Triangular Nanoprisms: Correlating Scattering with Structure Using Electrodynamics for Plasmon Lifetime Analysis. *Journal of Physical Chemistry C* **2012**, *116* (1), 393–403.

List of Symbols, Abbreviations, and Acronyms

AFM	atomic form microscopy
Ag	silver
Au	gold
BPE	trans-1,2-bi-(pyridyl) ethylene
DARPA	Defense Advanced Research Projects Agency
EtOH	ethanol
KOH	potassium hydroxide
LOD	limits of detection
LSPR	localized surface plasmon resonance
NIR	near-infrared
RSD	relative standard deviation
SEM	scanning electron microscopy
SERS	surface enhanced Raman scattering
S/N	signal-to-noise

NO. OF COPIES	ORGANIZATION
1 ELEC	ADMNSTR DEFNS TECHL INFO CTR ATTN DTIC OCP
1 PDF	MIKELLA FARRELL U.S. ARMY RESEARCH LABORATORY RDRL-SEE-O
1 PDF	GARY WOOD U.S. ARMY RESEARCH LABORATORY RDRL-SEE
1 PDF	LINDA BLISS U.S. ARMY RESEARCH LABORATORY RDRL-SEE
1 PDF	US ARMY RSRCH LAB ATTN RDRL CIO LL TECHL LIB